Evolutionary adaptation after crippling cell polarization follows reproducible trajectories.

Liedewij Laan[1,*], John H. Koschwanez[1], Andrew W. Murray[1].

[1]FAS Center for Systems Biology and Department of Molecular and Cellular Biology, Harvard University, Cambridge, United States;

[*] Current address: Bionanoscience Department, Delft University of Technology, the Netherlands.

Abstract

Cells are organized by functional modules, which typically contain components whose removal severely compromises the module's function. Despite their importance, these components are not absolutely conserved between parts of the tree of life, suggesting that cells can evolve to perform the same biological functions with different proteins. We evolved *Saccharomyces cerevisiae* for 1000 generations without the important polarity gene *BEM1*. At the end of the evolution the *bem1*Δ lineages rapidly increase in fitness and then slowly reach >90% of the fitness of their *BEM1* ancestors. Sequencing their genomes and monitoring polarization reveals a common evolutionary trajectory, with a fixed sequence of adaptive mutations, each improving cell polarization by inactivating proteins. Our results show that organisms can be evolutionarily robust to physiologically destructive perturbations and suggest that recovery by gene inactivation can lead to rapid divergence in the parts list for cell biologically important functions.

Introduction

Advances in cell biology, genetics, and systems biology have led to substantial understanding of how cells perform complex tasks precisely. In cell polarization and movement, a biochemical and biophysical picture is emerging of how those complex functional modules self-organize to accomplish their functions [1, 2]. Surprisingly, components that are essential for a module in well-studied model organisms can be absent in evolutionarily distant organisms [3], even though the modules must perform the same tasks. This observation suggests that complex modules reorganize during evolution, either to accommodate changing requirements, or to respond to the chance loss of components during population bottlenecks, when selection against deleterious mutations is greatly diminished.

One approach to understanding the evolution of functional modules is to compare them between different species [4-6]. In closely related, inter-fertile species, genetic analysis can reveal the mutations that account for functional differences, but not their temporal order, and even this level of detail cannot be achieved in more distantly related species. Experimental microbial evolution circumvents these problems: sequencing and genetic analysis identifies the mutations responsible for the selected phenotype and storing and analyzing intermediate steps reveals the order in which mutations occurred [7, 8]. In principle, these tools should lead to mechanistic understanding of evolutionary trajectories, but selections for faster growth or novel functions typically produce adaptive mutations in multiple functional modules [9], whose relationship to each other is hard to explain. Are there multiple solutions to the selection, resulting in independent additive solutions in different cellular modules [10, 11], or are those mutations (and the modules they lay in) coupled in an unknown way [12]?

We focused selective pressure by allowing populations to evolve after deleting an important gene in a well-described module. This approach differs from traditional suppressor screens, which isolate single compensatory mutations, by selecting for combinations of mutations, which together significantly increase fitness. The module we perturbed was polarization in budding yeast [13-20]. Polarization involves selection of an axis of polarity, followed by the asymmetric organization of cytoskeletal elements and membranous organelles and cell wall growth along this axis. Yeast cells polarize and bud by localizing and activating the small GTPase, Cdc42, at a single site [20, 21]. In haploid cells, polarization is directed by a historical mark deposited in the previous cell cycle, but even when the mark is absent, yeast cells still polarize efficiently, albeit at a random location [22]. Under these conditions, symmetry breaking depends on at least two pathways: 1) an actin-based mechanism based on the positive feedback between actin-mediated delivery of Cdc42 to the plasma membrane and actin polymerization stimulated by membrane-bound Cdc42 [18, 23-25], and 2) an actin-independent, Turing type mechanism that depends on interactions amongst proteins that regulate the activity and localization of Cdc42 [13, 18, 26] (Figure 1A). We strongly perturbed yeast polarization by removing Bem1, a regulator of Cdc42, which recruits the guanine exchange factor (GEF) Cdc24 as well as Cdc42 to the membrane where Cdc24 activates membrane bound Cdc42. We decided to delete Bem1 because previous research suggests that this protein is a relatively young component in polarity establishment that had a different role in ancestral fungi [27]. Deleting this component of polarity could thus reveal other alternative, more evolutionarily ancient polarization modules.

Deleting Bem1 led to profound defects in cell polarization and proliferation, but cells recovered to nearly wild-type growth rates over 1000 generations. Genetic analysis revealed that this recovery followed a reproducible trajectory in which the same genes, which regulate polarization, were inactivated in the same order. Systematic analysis of the interactions between the mutated genes revealed epistatic interactions that explained the evolutionary trajectory that gradually improved cell polarization. We discuss the role of loss of function mutations in the evolution of populations outside the laboratory.

Results

Rapid evolution in *bem1*Δ lineages

We started by constructing *bem1*Δ cells, in the W303 strain background, by sporulating a heterozygous *BEM1/bem1*Δ diploid. *bem1*Δ spores formed colonies at a frequency of $6\pm0.4\text{x}10^{-5}$ (Figure 1B, for details see Supplementary Materials), while wild-type (*BEM1)* spores formed colonies at a frequency of 0.95. We imaged *bem1*Δ and wild-type spores as they germinated and followed several subsequent cell divisions (Video 1), where we measured the time of budding as a proxy for polarization: cells cannot bud without a successful polarization event. The majority of *bem1*Δ cells (28/35 versus 0/41 for wild-type cells) did not polarize within 500 min but grew isotropically resulting in very large cells (Figure 1C) that often lysed (16/35) (Video 2). The *bem1*Δ cells that did polarize, (Figure 1D, $P_{polarize\_bem1\Delta}$=0.23, N=35), polarize fast, in contrast to wild type cells, which show a wider distribution of polarization times, but always eventually polarize successfully (Figure 1D, $P_{polarize\_wt}$=1, N=41).We used a single *bem1*Δ colony, as well as a control, wild-type colony, as the starting point for our evolution experiments. From both colonies, we started with ten wild-type

and ten *bem1*Δ cultures, which we evolved for one thousand generations by serial dilutions, regularly freezing down a sample (Figure 2A and see Supplementary Materials), resulting (due to contamination) in nine surviving *bem1*Δ lineages and seven wild-type lineages. We characterized their phenotypic trajectories by measuring the population growth rate at different time points. The initial growth rate of the *bem1*Δ lineages was approximately 12 times lower than the wild-type growth rate. By the end of the experiment, however, the *bem1*Δ cells grew at almost the rate of their wild-type ancestors. (Figure 2B). Two *bem1*Δ lines, A1 and A2, are plotted individually because they are discussed in more detail later in the paper, and one line, A8, became diploid and was excluded from further analysis. We examined how the cell size distribution, which is an approximation for polarization dynamics (Figure 2 - figure supplement 1E), changed during the experiment: cells that take longer to polarize are on average larger than cells that polarize fast because yeast cells continue to grow during polarity establishment [28]. We measured cell size distributions (Figure 2D, see Supplementary Materials) and fitted them to a log normal distribution to determine the mode, as a measure of the dominant cell size, and standard deviation, which we take as an approximation for noisiness in polarization dynamics. At the beginning of the experiment, *bem1*Δ cells were larger and showed a wider distribution than the wild-type ancestor (Figure 2CEF) as confirmed by microscopy (Figure 1 – figure supplement 1, Figure 1 and Figure 2D). At the end of the experiment, however, both the mode and the standard deviation in *bem1*Δ cells adapted to wild-type cell size (Figure 2D) and growth rate values, suggesting a properly functioning polarization machinery.

Reproducible evolutionary trajectories in parallel lineages

Which mutations caused the changes in growth rate and cell size? We sequenced the whole genomes of several evolved lines: From the seven wild-type lines that were left at the end of the evolution experiment, we sequenced five lines. We sequenced a total of ten *bem1*Δ lines: The eight bem1Δ A-lines that arose from the same starting colony and remained haploid, as described above. In addition, we sequenced two *bem1*Δ lines that were evolved from two independent different starting colonies in a trial experiment (T2 and T3). In the control, wild-type lines we found a diverse set of mutations (Supplementary File 1), with only one gene, *ECM21*, being mutated twice. *ECM21* was also the only mutated gene, in our control lines, that was also found in either of two other large scale evolution experiments [7, 29], suggesting that adaptation in our control experiments involves similar mutations to those in other studies that have led to modest increases in the proliferation rate of wild-type cells. This is in contrast to the mutations we found in the ten *bem1*Δ lines. We found three genes that were mutated at least three times: *BEM3* (10/10), *NRP1* (5/10) and *BEM2* (3/10). Mutations in these genes were not reported in a variety of other yeast evolution experiments [7, 9, 10, 29, 30], suggesting that they are specific for the deletion of *BEM1*. All other mutations can be found in Supplementary File 1. Only one of these mutations, the mutation in *IRA1*, in line T3, is also commonly found in other yeast evolution experiments suggesting it is not specific for the deletion of *BEM1*(Figure 3A). The A-lines shared the same early stop mutation in *BEM3*, but lines T2 and T3 independently acquired a different early stop mutations in *BEM3*. The *BEM3* mutation in the A-lines (Q61*) was acquired after germination of the spore that acted as their ancestor: cells from the original colony showed the same severe growth defects as freshly germinated *bem1*Δ spores, whereas engineered *bem1*Δ *bem3*Δ cells had a much less severe defect. All five mutations in *NRP1* (all in A-lines) were independently

147 acquired early stop mutations, whereas in *BEM2* we found a promoter mutation (line
148 T2) and two amino acid substitutions (line A1 and A2), which are radical substitutions at
149 conserved positions.

150 Lines A1 and A2 acquired mutations in *BEM2, BEM3* and *NRP1*. Sanger
151 sequencing of the three genes at different time points revealed that those mutations
152 occurred sequentially in *BEM3*, *NRP1*, and *BEM2* in both lines (Figure 3B). We
153 investigated whether this order was coincidental or caused by epistasis, by
154 investigating the phenotypes of mutations in these three genes, in different
155 combinations, in a *bem1*Δ background. We approximated the mutations by gene
156 deletions, assuming that the evolved mutations had eliminated (in the case of nonsense
157 mutations) or diminished (amino acid substitutions) gene function. We generated the
158 different genotypes by sporulating a *BEM1/bem1*Δ *BEM2/bem2*Δ *BEM3/bem3*Δ
159 *NRP1/nrp1*Δ diploid *(*Figure 3 – figure supplement 1A*)*. For each genotype, we
160 measured the average colony size generated by germinating spores, the percentage of
161 spores that produced visible colonies, and the growth rate in liquid media (Figure 3E,
162 Figure 3 - figure supplement 1B, C). Figure 3C shows that *bem1*Δ spores are least
163 likely to form colonies, while *bem1*Δ *bem2*Δ *bem3*Δ *nrp1*Δ spores closely resemble
164 wild-type spores, confirming that inactivating *BEM2*, *BEM3,* and *NRP1* substantially
165 suppresses the severe polarization defect of *bem1*Δ cells. We compared the growth rate
166 of quadruply mutant *bem1*Δ *bem2*Δ *bem3*Δ *nrp1*Δ cells with the final populations of
167 line A1 and A2 (Fig. 3D). The growth rate of line A2 is indistinguishable from the
168 reconstructed strain, which carries gene deletions in the genes that were mutated in our
169 experiments, suggesting we found the mutations that confer fitness to this lineage, but
170 line A1 grows slightly faster than the quadruple mutant, suggesting it may contain
171 additional adaptive mutations.

What does the successful reconstruction tell us? First it reveals epistasis, in particular sign epistasis (a mutation switching from being beneficial to deleterious) for some combinations of mutations. If mutations are added in the order they occurred in during the evolution, each successive mutation increases the fitness of the resulting strain, but adding mutations in different orders can reduce fitness. (Figure 3C): adding the *bem2*Δ mutation increases the growth rate of *bem1*Δ *bem3*Δ *nrp1*Δ cells, but the same mutation reduces or has no effect on the fitness of all other tested genotypes. Another example of epistasis is the changing dependence of the cells on *BEM1*: the polarization module evolves from requiring Bem1, in wild type strains, to being slightly impaired by the presence of functional Bem1 in a *bem2*Δ *bem3*Δ *nrp1*Δ mutant (Figure 3D).

Adaptive mutations alter the dynamics of cell polarization

Reconstruction allowed us to examine how different combinations of mutations alter the dynamics of the polarization module. Because there are large cytoplasmic pools of Cdc42, which make it hard to monitor the location of membrane-associated, active Cdc42, we examined polarization by imaging Spa2-Citrine, which localizes to the polarity site and the cytokinetic ring (Figure 4AB, Video 4) [31]. We measured two parameters: $t_{fs\text{-}c}$, the average time between cytokinesis t_c and the appearance of the first polarity site t_{fs}, and how long cells spent with zero, one, two or three polarity sites in the interval between the appearance of the first focus of Spa2-Citrine and budding. As expected, *bem1*Δ cells have a long delay before the first signs of polarization, and polarization is often abortive (Video 5, Figure 4C), suggesting weaker activation of Cdc42. In addition, *bem1*Δ cells often contain more than one polarity site, suggesting that the positive feedback that ensures a single site of polarization is weaker.

196 The nature of the mutated genes suggests how inactivating them improves the
197 polarization of *bem1*Δ cells. *BEM3* and *BEM2* encode two of the four GAPs (GTPase
198 Activating Proteins) in the polarity module that inactivate Cdc42 [32] and other small
199 G proteins by stimulating their intrinsic GTPase activity. Inactivating these genes
200 should increase Cdc42 activity. As predicted, *bem1*Δ*bem3*Δ cells bud faster (Video 6,
201 Figure 4C), but the cells still often contain more than one polarity site, suggesting that
202 increasing Cdc42 activity is not enough to re-establish precise positive feedback in the
203 absence of Bem1.

204 Less is known about *NRP1,* an RNA binding protein that localizes to stress
205 granules and has not been related to polarity before [33]. A high-throughput RNA
206 binding study suggested seven target RNAs for *NRP1,* but none of them forms an
207 obvious link to polarity, and most have an unknown function [34]. The most obvious
208 change after *NRP1* deletion is a decrease in time between cytokinesis and the
209 appearance of the first polarity site (Video 7, Figure 4C). Therefore we speculate that
210 *NRP1* plays a role in initiating polarization, which is triggered when Cdc28 is
211 activated by G1 cyclins. Cdc28 activation releases Cdc24 from the nucleus, activating
212 Cdc42. If the absence of Nrp1 leads, directly or indirectly, to the release of more
213 Cdc24, this would lead to faster activation of Cdc42 and earlier polarization. Finally,
214 the loss of Bem2 reduces the time that the cells are not polarized, suggesting this
215 mutation also increases Cdc42 activity (Video 8).

216 Our data suggests that that multiple mutations can restore Cdc42 activity
217 without restoring Bem1's ability to physically connect Cdc24 and Cdc42. As a
218 consequence, actin-based positive feedback, which only requires Bem1 to activate
219 Cdc42, will become critical because actin independent-polarization depends directly
220 on Bem1 acting as a scaffold. Previous work showed that when actin-based positive

feedback acts alone, it creates multiple simultaneous polarity sites [18], as we observe in our mutants.

Discussion

We followed the evolutionary adaptation to the removal of an important component of the module that polarizes budding yeast cells. Cells recovered by following a reproducible evolutionary trajectory that could be largely explained by the interactions amongst the mutated genes and led to a substantial recovery in the speed and accuracy of cell polarization.

How repeatable is evolution? Experimental evolution has produced a range of answers to this question, from replicate populations that share a small fraction of causal mutations[10, 29, 30, 35] to those where mutations occur in the same genes in the same order [36, 37] or repeatedly affect the same amino acids in a protein [38]. For multiple substitutions in the same protein, strong epistasis can render most trajectories impossible or unlikely [39-41]. Examining the mutations that gave rise to a particular phenotype in the bacterium, *Pseudomonas fluorescens*, revealed a hierarchy of pathways: loss of function mutations are most frequent and other pathways, including promoter mutations, gene fusions, and gain of function mutations can only be found when the dominant pathway is blocked [42].

Our work adds to the list of examples of reproducible trajectories and our reconstruction of all possible paths, an exercise that has previously been performed for multiple mutation in a single gene [41], demonstrates why our mutations occurred in a particular order. As far as we know, this is the first example of reproducible trajectories to adaptation to mutations that severely compromise a cellular function,

and it will be interesting to see if evolving strains, adapting to severe perturbations in other pathways will also lead to reproducible trajectories.

We interpret our results as demonstrating that the multiple layers of regulation that allow cells to polarize rapidly and accurately also make it possible for them to adapt, by evolution, to very strong perturbations. Under strong selective pressure, the larger target size for mutations that inactivate proteins favors evolutionary trajectories that remove components from modules over those that quantitatively alter their properties. As long as modules contain components, like Bem2 and Bem3, which alter the quantitative behavior of other proteins, like Cdc42 and other small GTPases, removing the regulators is the equivalent of rarer mutations that would change the biochemical parameters of central components of the pathway. Our findings are consistent with previous experimental evolution work which showed that loss of function mutations allow bacteria [43, 44] and yeast [10] to adapt to their environments and produce novel phenotypes [12]. Adaptation by loss of function mutations has also been observed in natural populations [45-49].

In our work, the selected mutations do not alter the structure of an existing protein to allow it to play Bem1's role of physically linking Cdc42 to Cdc24. Instead, other mutations that increase the half-life of Cdc42-GTP (and possibly other small G proteins) remove the need to hold Cdc24 and Cdc42 close to each other. We suspect that the differing effects of removing genes and altering gene dosage may control the type of mutations that allow cells to adapt to large genetic perturbations. If increasing the dosage of genes can reverse the effects of the perturbation, cells may recover by becoming aneuploid, as observed when duplicating chromosome XVI increases the dosage of two genes (*MKK2* and *RLM1*) that help compensate for the absence of type II myosin [50]. In contrast, if removing inhibitors will increase fitness, point mutations

that inactivate the inhibitors will be selected, as we observed. Investigating how cells recover from other perturbations in these and different pathways will test the validity of this speculation, reveal the mechanistic details underlying evolutionary change, and improve our understanding of how the self-organizing properties of modules affect the course of evolution.

Our results may help to explain the surprising observation that certain eukaryotic lineages lack extremely well conserved pathways, such as the absence of the anaphase promoting complex from Giardia [51] or conserved kinetochore proteins from kinetoplasids [52]. Although less in known about the evolutionary history of polarity proteins, recent studies suggest that the components of this pathway also vary substantially. In filamentous fungi, Cdc42 is not essential because its function is shared with Rac1[53]. However, the deployment of Cdc42 module and Rac1 module for critical morphogenetic functions is surprisingly different between closely related species [54]. Our study shows that removing one component of a conserved pathway selects for the inactivation of others. If this process was accompanied by the recruitment of novel proteins, it could ultimately lead to an evolutionary shift that replaced one module with another unrelated one that performed the same function.

One objection to this hypothesis is that it would be very hard to fix a mutation as deleterious as *bem1*Δ. There are ways of countering the objection: severely defective mutations could be fixed in population bottlenecks that accompany speciation; secondly, and maybe more likely, mutations that removed important components could be pleiotropic, offering advantages in novel environments that were similar in magnitude to the costs they impose on strongly conserved core functions; and thirdly, previously selected mutations in the same or related pathways could make the defects associated with the removal of a component less severe.

294 Because of the difficulty of inferring events as ancient as the ones that
295 rearranged the kinetochore of kinetoplastids or made the anaphase promoting complex
296 dispensable in *Giardia*, it is impossible to say whether it was the loss of genes that
297 inactivated existing pathways, or some other event that triggered the sequence of
298 changes that led particular lineages to use different proteins to perform functions that
299 appeared early in eukaryotic evolution. Despite our inability to reconstruct these
300 processes, there is evidence for individual steps in the process of functional
301 reorganization. These include the loss of widely conserved genes in individual
302 evolutionary lineages [3, 51, 55], the loss of genes present in ancestral species during
303 evolutionary diversification (e.g. the loss of 88 genes in the descent of *S. cerevisiae*
304 from an ancestor that existed 100 Mya ago [56]), and the recruitment of new functions
305 by adaptations that alter the function of existing genes and create genes de novo[57,
306 58].

307 Our evolution experiment created a related set of rapid polarizing mechanisms.
308 Deciphering the physical mechanisms of polarity establishment in all the different
309 combinations of mutants will teach us about evolution of functional modules.
310 However, it will also reveal more about cell biology of polarization. First, it can help
311 to identify the role of new genes in polarity establishment; previous work has
312 implicated Nrp1 in RNA binding, ribosome biogenesis, and the formation of stress
313 granules, whereas our experiments demonstrate that it regulates cell polarization,
314 directly or indirectly. High throughput studies, at least as indicated on the yeast
315 genome website SGD [59] have not shown physical or genetic interactions between
316 *NRP1* and any of the currently known polarity genes [59]. *BEM1*, *BEM2* and *BEM3* as
317 well as their genetic interactions have been measured and implicated in polarity establishment
318 before [60]. However, the lack of information about *NRP1* made it impossible to predict the

positive effect of the *BEM2* deletion on polarity establishment in the absence of *BEM1* and *BEM3*.

Second, by biophysically investigating how cells recover from the deletion of *BEM*1 as well as other perturbations in the polarity pathway, we will be able to distill which parts of polarization mechanisms, rather than molecules, are essential for proper function. Cell polarization is a complicated, dynamical process, thus it may be more important to alter quantitative parameters of the overall process, regardless of the gene whose mutation produces the change, than it is to alter the behavior of a particular protein.

Materials and methods

Yeast strains/ Media: The W303 strain background was used for all experiments. Supplementary File 2 provides a detailed list of each strain used. Standard rich media, YPD (2% Peptone, 2% D–Glucose and 1% Yeast-Extract) was used for the evolution experiments. For the microscopy experiments non-fluorescent yeast media was used, which was prepared from refrigerated 10× yeast nitrogen base (YNB), 20% D–Glucose (10x), and sterilized water. The amino acids leucine, histidine and uracil were added from a 100x stock. The YNB was based on the recipe of Wickerham [62], with the following modifications: riboflavin and folic acid were not added to the YNB to minimize auto fluorescence [63]. All other media was prepared according to [64].

Generating the various mutant haploid cells (Figure 1B, Figure 3C): The various haploid strains in our study were generated by sporulating heterozygous diploids. This approach allowed us to select and monitor barely viable mutants from the moment they were created, and allowed us to observe the occurrence of the first and subsequent suppressor mutations. Diploid strains were sporulated in liquid culture by growing them to saturation in YPD at

343 30°C. Afterwards they were diluted into YEP (2% Peptone and 1% Yeast-Extract) with 2%
344 potassium acetate for 12 hours at 30°C, washed with water, resuspended in 2% potassium
345 acetate and grown at 25°C for 3-5 days. The sporulation efficiency was checked under the
346 microscope. If the sporulation efficiency was high enough (>95%) 1.5 ml of spores were spun
347 down, resuspended in 500 µl Zymolyase solution (10ug/ml Zymolyase in TE (10 mM Tris, 1
348 mM EDTA, pH 7.5) and incubated at 36°C for 60 minutes, to digest the ascus. Afterwards the
349 spores were spun down, resuspended in 500 µl 0.1% SDS + 0.1% Triton in TE and incubated
350 at 36°C for 30 min, to disrupt the membranes of remnant diploid cells. Subsequently the
351 spores were vigorously vortexed and the spore concentration was measured with a Coulter
352 Counter (Z2 analyser; Beckman Coulter, Inc., Danvers, MA). 10^1, 10^2, and 10^3 spores were
353 plated on YPD plates (3x per condition), to get an estimate of the total number of viable
354 spores. To select for viable *bem1*Δ cells (Figure 1), 10^3, 10^4 , 10^5 and 10^6 spores were also
355 plated on 4xG418/10xCANAVINE/-HIS plates (3x per condition), which we will refer to as
356 the selection plates. The selection plate strongly selected for *MAT***a**-haploid spores [61] that
357 lack *BEM1*: the absence of histidine selects for haploid *MAT***a** strains, because the *MFA1*
358 promoter is expressed only in **a** cells, the presence of canavanine is a second selection for
359 haploids, since the *CAN1* gene dominantly confers sensitivity to canavanine, an arginine
360 analog, and G418 selects for *bem1*Δ because the gene deletion is marked with the bacterial
361 kanamycin resistance gene. After 2 days, the colonies on the YPD plates were counted and
362 used to normalize the number of colonies on the selection plate to calculate the survival
363 probability. The error is the standard deviation between five independent experiments and
364 includes the statistical plating error.

365 **Characterizing *bem1*Δ mutants (Figure 1CD):** The colonies that grew on the selection
366 plates were checked for the absence of *BEM1* by PCR (later this was confirmed by whole
367 genome sequencing). Typically ~20% of the colonies were indeed *bem1*Δ. The other cells

were most likely haploid, *MAT***a**, cells, aneuploid for chromosome II and thus contained both *BEM1* and the selection marker. Cells from a confirmed *bem1*Δ colony were used to start the evolution experiments. In addition, some cells from the same colony were imaged every 3 min for several hours with a Ti-E inverted microscope (Nikon), with a Perfect Focus system and a 60x DIC oil objective (figure supplement 1) while being confined in an agar pad. Germinating *bem1*Δ*,* as well as wild-type spores were imaged every 3 minutes for 20 hours in the same microscope but in a micro fluidic chamber (CellAsic, Millipore) to allow for constant media supply. The time between cytokinesis and bud formation for mothers was manually determined. Only mothers were analysed to minimize the effect of cell size on the time between cytokinesis and bud formation.

Experimental evolution experiments (Figure 2A): The evolution experiments were initiated with 10 *bem1*Δ (A-lines) and 10 wild-type cultures (3aA-lines). The 10 *bem1*Δ cultures were derived from the same starting colony, and the 10 wild-type colonies were derived from an individual colony from the yLL3a strain. The individual colonies were dissolved into 1 ml YPD media and counted. Every independent 10 ml YPD culture was inoculated with 10^6 cells. The glass tubes were placed in a roller drum at 30^{o}C. On the vast majority of days, we checked the culture density in the morning (10am +/- 1 hour). If the culture density was $<5.10^7$ cell/ml, the cells were grown for another 24 hours, otherwise it was passaged as follows. First, 10 µl of the culture was pipetted into 10 ml of fresh YPD and placed in a roller drum at 30^{o}C. Second, 1 ml of culture was mixed with 500 µl of 50% Glycerol in water and frozen at -80^{o}C. Initially cells were frozen down after every passage, however after passage 20 this was reduced to every 5 passages. Early in the evolution experiment 1 *bem1*Δ culture and 3 wild-type cultures were lost due to bacterial contamination. The other cultures were all evolved for 1000 generations (100 passages), except for line A2 which got contaminated after

33 passages, but was restarted from the frozen stock at passage 30 and was evolved for 820 generation (82 passages).

As a pilot experiment, two *bem1*Δ cultures (T2 and T3) were evolved for 1000 generations according to the same protocol, with the exception that they were taken from independent colonies.

Growth rate measurements and analysis (Figure 2B): The population growth rate was measured at different time points during the evolution experiments. Approximately 10^5 cells were taken from the frozen stock and inoculated in 2 ml of YPD. We used YPD from the same batch for the complete evolution experiment as well as for the analysis of the evolution experiment. The cultures were incubated on a roller drum at 30˚C overnight and the next morning the growth rate in log phase was measured by taking several time points with a Coulter Counter and fitting the data to an exponential function with a home written program in Matlab. For every data point, at least three independent experiments were used. The error bar indicates the standard deviation between the different experiments.

Cell size measurements and analysis (Figure 3DEF): In addition to the growth rate, the population cell size distribution was measured at different time points during the evolution. Approximately 10^5 cells were inoculated from the frozen stock into 2-5 ml of YPD; for each condition, three independent cultures were started in parallel. The cells were grown overnight in a roller drum at 30^{o}C to reach log phase in the morning. If the cell density was $>4x10^6$ and $< 3x10^7$ a sample 50 µl of cells was diluted into 20 ml of Coulter Counter isotone solution. Subsequently the cuvettes were sonicated on ice for 20 secs, to reduce clumpiness. Afterwards 100,000 particles were measured with the Beckman Coulter Multisizer 3. For most conditions, three independent experiments were performed (typically consisting of three independent cultures). The distribution of cells sizes measured was imported in Matlab and fitted with a

log-normal distribution to obtain the mode and the standard deviation. The error bars are the standard deviations between different cultures

Whole genome sequencing and analysis (Supplementary File 1): Genomic DNA library preparation was performed as in [12] with an Illumina Truseq DNA kit on a Illumina Hiseq 2000 with 150 base paired end reads. The Burrows-Wheeler Aligner (bio-bwa.sourceforge.net) (Li and Durbin, 2009) was used to map DNA sequences to the *Saccharomyces cerevisiae* reference genome r64, which was downloaded from *Saccharomyces* Genome Database (www.yeastgenome.org). The samtools software package (samtools.sourceforge.net) was then used to sort and index the mapped reads into a BAM file. GATK (www.broadinstitute.org/gatk) (McKenna et al, 2010) was used to realign local indels, and Varscan (varscan.sourceforge.net) (Koboldt et al, 2012) was used to call variants. Mutations were found using a custom pipeline written in Python (www.python.org) using the Biopython (biopython.org) and pysam (github.com/pysam-developers/pysam) modules. The pipeline (github.com/koschwanez/mutantanalysis) [10] compares variants between the reference strain, the ancestor strain, and the evolved strains. A variant that occurs between the ancestor and an evolved strain is labelled as a mutation if it either (1) causes a non-synonymous substitution in a coding sequence, or (2) occurs in a promoter region, defined as 500 bp upstream of the coding sequence.

Analysis of allele frequency with sanger sequencing (Figure 3B): Commercial Sanger sequencing returns trace plots, chromatograms that indicate the relative frequency of each base at each position in the sequenced DNA. Trace plots were used to estimate the fraction of mutant alleles in a population at different time points during the evolution. The fraction of mutant alleles in the population was assumed to be the height of the mutant allele peak divided by the height of the mutant allele peak plus the ancestor allele peak. In the time course analysis, values below the approximate background level were assumed to be zero, and

values above 95% were assumed to be 100% [64]. In line A2 the dynamics of the mutant *bem2* and mutant *nrp1* allele are close in time. However two observations strongly indicate that the *bem2* mutation occurred after the *nrp1* mutation: (1) there is a consistent difference at different time points between the fraction of *nrp1* and *bem2* mutant alleles and (2) the difference between the fraction of the population that contain the *nrp1* and *bem2* mutant alleles at the final time point is confirmed by whole genome sequencing.

Generation and analysis of reconstructed strains (Figure 3CD, figure supplement 3BC): The various strains carrying gene deletions in the genes that were mutated in our experiments were generated by sporulation of a heterozygous diploid (yLL112a and yLL135a). The phenotype was determined by replica plating colonies that grew from single spores to all the different plates necessary to detect the different markers (figure supplement 3BC). Single spore colonies were generated by spotting individual spores with a FACS cell sorter (MoFlo Legacy, Dako Cytomation/Beckman Coulter)) on YPD plates. 81 spores were spotted per plate on a total of 10 plates. After two days, the plates were imaged to measure the colony size. Calibration experiments showed that in this period the colony size is a good approximation for the growth rate of the cells in the colony. Subsequently the colonies were replica plated to various drop-out and drug plates to determine their genotype. Home written software in Matlab was used to determine the colony size of every colony and to combine it with its genotype. From this data the average colony size per genotype and the standard deviation between the colony sizes was calculated. In addition the percentage of surviving colonies was calculated by diving the number of observed colonies by the number of expected colonies*100%. The error bar is the statistical error (% surviving colonies/$\sqrt{N}$, N is number of observed colonies). Comparing the wild-type data from assaying the behavior of the spores spotted on plates with results obtained from tetrad dissections of wild-type diploids, confirmed that the spore plotting assay did not introduce bias in the growth rates or fraction of

surviving colonies. The percentage of surviving *bem1*Δ colonies was higher in this assay than in the original assay (Figure 1AB), which we attribute to the presence of Spa2-Citrine: all the *bem1*Δ colonies that survived contained Spa2-Citrine, even though this allele was heterozygous in the diploid that they were derived from. After replica plating, approximately 10^5 cells/genotype were inoculated into 2 ml YPD and incubated on 30^{o}C on a roller drum overnight and the next morning the growth rate in log phase was measured by taking several time points with a coulter counter and fitting the data to an exponential function with a home written program in Matlab. For every data point, typically three independent experiments were used. The error bar indicates the standard deviation between different experiments

Fluorescence microscopy of reconstructed strains (Figure 4A): The polarization dynamics of the reconstructed strains were measured by imaging Spa_Citrine, a polarity marker, present in the reconstructed strains. Cells were grown to log phase and flowed into in a microfluidic culture chamber, which allowed for constant culturing conditions (CellAsic, Millipore). The cells were maintained in log-phase by constantly supplying non-fluorescent growth media. Images were taken with a 60X objective on a Nikon inverted Ti-E microscope with a Yokagawa spinning disc unit and an EM-CCD camera (Hamamatsu ImagEM); Citrine was excited with a 488 nm laser; exposure times were 200 msecs with a time interval of 2 or 3 minutes. Typically 16 positions were imaged for 8 hours per experiment. At each location a z-stack was taken with 7 z-steps of 1 μm. For analysis, a movie was created from maximum projections of these z-stacks. For every mutant (Figure 4), two independent experiments (consisting of at least 4 different locations) were analyzed.

Data analysis of fluorescence microscopy of reconstructed strains (Figure 4C): For every mother cell between cytokinesis and bud take off, we manually determined, at each frame, how many Spa2 spots were present. Only mothers were considered to minimize the effect of cell size on the data. The time between cytokinesis and the first spot and the time between the

first spot and bud appearance were analysed separately. From this data the average total time per cell cycle that cells contain zero, one, two or three polarity spots was calculated.

Author contributions: LL and AWM designed the research. LL performed the research and analysed the data. JHK performed whole genome sequence analysis. LL and AWM wrote the paper.

Acknowledgements:

We thank the Boeke lab for providing us with the magic marker, G. Wildenberg for help with cell sorting, M. Coelho and P. Hsieh for help with library generation, Bertus Beaumont, Michael Desai, Vlad Denic, Cassandra Extavour, Michael Laub, and Melanie Mueller for critical reading of the manuscript, R. Wedlich-Soldner and members of the Murray and Nelson labs for useful discussions. This work was supported by grant GM06783 from the National Institute of General Medical Sciences. LL gratefully acknowledges support from the Netherlands Organization for Scientific Research through a Rubicon grant, as well as from the Human Frontiers Science Program through a cross disciplinary post-doctoral grant.

References

1. Goehring, N.W. and S.W. Grill, *Cell polarity: mechanochemical patterning.* Trends Cell Biol, 2013. **23**(2): p. 72-80.
2. Howard, J., S.W. Grill, and J.S. Bois, *Turing's next steps: the mechanochemical basis of morphogenesis.* Nat Rev Mol Cell Biol, 2011. **12**(6): p. 392-8.
3. Bergmiller, T., M. Ackermann, and O.K. Silander, *Patterns of evolutionary conservation of essential genes correlate with their compensability.* PLoS Genet, 2012. **8**(6): p. e1002803.
4. Azimzadeh, J., et al., *Centrosome loss in the evolution of planarians.* Science, 2012. **335**(6067): p. 461-3.
5. Carvalho-Santos, Z., et al., *Evolution: Tracing the origins of centrioles, cilia, and flagella.* J Cell Biol, 2011. **194**(2): p. 165-75.
6. Vleugel, M., et al., *Evolution and function of the mitotic checkpoint.* Dev Cell, 2012. **23**(2): p. 239-50.
7. Lang, G.I., et al., *Pervasive genetic hitchhiking and clonal interference in forty evolving yeast populations.* Nature, 2013. **500**(7464): p. 571-4.

8. Lenski, R.E. and M. Travisano, *Dynamics of adaptation and diversification: a 10,000-generation experiment with bacterial populations.* Proc Natl Acad Sci U S A, 1994. **91**(15): p. 6808-14.
9. Kvitek, D.J. and G. Sherlock, *Whole genome, whole population sequencing reveals that loss of signaling networks is the major adaptive strategy in a constant environment.* PLoS Genet, 2013. **9**(11): p. e1003972.
10. Koschwanez, J.H., K.R. Foster, and A.W. Murray, *Improved use of a public good selects for the evolution of undifferentiated multicellularity.* Elife, 2013. **2**: p. e00367.
11. Khan, A.I., et al., *Negative epistasis between beneficial mutations in an evolving bacterial population.* Science, 2011. **332**(6034): p. 1193-6.
12. Wildenberg, G.A. and A.W. Murray, *Evolving a 24-hr oscillator in budding yeast.* Elife, 2014. **3**.
13. Howell, A.S., et al., *Negative feedback enhances robustness in the yeast polarity establishment circuit.* Cell, 2012. **149**(2): p. 322-33.
14. Kuo, C.C., et al., *Inhibitory GEF phosphorylation provides negative feedback in the yeast polarity circuit.* Curr Biol, 2014. **24**(7): p. 753-9.
15. Slaughter, B.D., et al., *Dual modes of cdc42 recycling fine-tune polarized morphogenesis.* Dev Cell, 2009. **17**(6): p. 823-35.
16. Gong, T., et al., *Control of polarized growth by the Rho family GTPase Rho4 in budding yeast: requirement of the N-terminal extension of Rho4 and regulation by the Rho GTPase-activating protein Bem2.* Eukaryot Cell, 2013. **12**(2): p. 368-77.
17. Smith, G.R., et al., *GTPase-activating proteins for Cdc42.* Eukaryot Cell, 2002. **1**(3): p. 469-80.
18. Freisinger, T., et al., *Establishment of a robust single axis of cell polarity by coupling multiple positive feedback loops.* Nat Commun, 2013. **4**: p. 1807.
19. Klunder, B., et al., *GDI-mediated cell polarization in yeast provides precise spatial and temporal control of Cdc42 signaling.* PLoS Comput Biol, 2013. **9**(12): p. e1003396.
20. Wu, C.F. and D.J. Lew, *Beyond symmetry-breaking: competition and negative feedback in GTPase regulation.* Trends Cell Biol, 2013. **23**(10): p. 476-83.
21. Slaughter, B.D., S.E. Smith, and R. Li, *Symmetry breaking in the life cycle of the budding yeast.* Cold Spring Harb Perspect Biol, 2009. **1**(3): p. a003384.
22. Chant, J. and I. Herskowitz, *Genetic control of bud site selection in yeast by a set of gene products that constitute a morphogenetic pathway.* Cell, 1991. **65**(7): p. 1203-12.
23. Marco, E., et al., *Endocytosis optimizes the dynamic localization of membrane proteins that regulate cortical polarity.* Cell, 2007. **129**(2): p. 411-22.
24. Slaughter, B.D., et al., *Non-uniform membrane diffusion enables steady-state cell polarization via vesicular trafficking.* Nat Commun, 2013. **4**: p. 1380.
25. Wedlich-Soldner, R., et al., *Spontaneous cell polarization through actomyosin-based delivery of the Cdc42 GTPase.* Science, 2003. **299**(5610): p. 1231-5.
26. Smith, S.E., et al., *Independence of symmetry breaking on Bem1-mediated autocatalytic activation of Cdc42.* J Cell Biol, 2013. **202**(7): p. 1091-106.
27. Semighini, C.P. and S.D. Harris, *Regulation of apical dominance in Aspergillus nidulans hyphae by reactive oxygen species.* Genetics, 2008. **179**(4): p. 1919-32.
28. Goranov, A.I., et al., *The rate of cell growth is governed by cell cycle stage.* Genes Dev, 2009. **23**(12): p. 1408-22.
29. Kryazhimskiy, S., et al., *Microbial evolution. Global epistasis makes adaptation predictable despite sequence-level stochasticity.* Science, 2014. **344**(6191): p. 1519-22.

30. Kvitek, D.J. and G. Sherlock, *Reciprocal sign epistasis between frequently experimentally evolved adaptive mutations causes a rugged fitness landscape.* PLoS Genet, 2011. **7**(4): p. e1002056.
31. Snyder, M., *The SPA2 protein of yeast localizes to sites of cell growth.* J Cell Biol, 1989. **108**(4): p. 1419-29.
32. Zheng, Y., R. Cerione, and A. Bender, *Control of the yeast bud-site assembly GTPase Cdc42. Catalysis of guanine nucleotide exchange by Cdc24 and stimulation of GTPase activity by Bem3.* J Biol Chem, 1994. **269**(4): p. 2369-72.
33. Buchan, J.R., D. Muhlrad, and R. Parker, *P bodies promote stress granule assembly in Saccharomyces cerevisiae.* J Cell Biol, 2008. **183**(3): p. 441-55.
34. Hogan, D.J., et al., *Diverse RNA-binding proteins interact with functionally related sets of RNAs, suggesting an extensive regulatory system.* PLoS Biol, 2008. **6**(10): p. e255.
35. Chou, H.H. and C.J. Marx, *Optimization of gene expression through divergent mutational paths.* Cell Rep, 2012. **1**(2): p. 133-40.
36. Blount, Z.D., et al., *Genomic analysis of a key innovation in an experimental Escherichia coli population.* Nature, 2012. **489**(7417): p. 513-8.
37. Herron, M.D. and M. Doebeli, *Parallel evolutionary dynamics of adaptive diversification in Escherichia coli.* PLoS Biol, 2013. **11**(2): p. e1001490.
38. Meyer, J.R., et al., *Repeatability and contingency in the evolution of a key innovation in phage lambda.* Science, 2012. **335**(6067): p. 428-32.
39. Bridgham, J.T., E.A. Ortlund, and J.W. Thornton, *An epistatic ratchet constrains the direction of glucocorticoid receptor evolution.* Nature, 2009. **461**(7263): p. 515-9.
40. Hinkley, T., et al., *A systems analysis of mutational effects in HIV-1 protease and reverse transcriptase.* Nat Genet, 2011. **43**(5): p. 487-9.
41. Weinreich, D.M., et al., *Darwinian evolution can follow only very few mutational paths to fitter proteins.* Science, 2006. **312**(5770): p. 111-4.
42. Lind, P.A., A.D. Farr, and P.B. Rainey, *Experimental evolution reveals hidden diversity in evolutionary pathways.* Elife, 2015. **4**.
43. Hottes, A.K., et al., *Bacterial adaptation through loss of function.* PLoS Genet, 2013. **9**(7): p. e1003617.
44. Zinser, E.R., et al., *Bacterial evolution through the selective loss of beneficial Genes. Trade-offs in expression involving two loci.* Genetics, 2003. **164**(4): p. 1271-7.
45. Bliven, K.A. and A.T. Maurelli, *Antivirulence genes: insights into pathogen evolution through gene loss.* Infect Immun, 2012. **80**(12): p. 4061-70.
46. D'Souza, G., et al., *Plasticity and epistasis strongly affect bacterial fitness after losing multiple metabolic genes.* Evolution, 2015. **69**(5): p. 1244-54.
47. D'Souza, G., et al., *Less is more: selective advantages can explain the prevalent loss of biosynthetic genes in bacteria.* Evolution, 2014. **68**(9): p. 2559-70.
48. Maurelli, A.T., et al., *"Black holes" and bacterial pathogenicity: a large genomic deletion that enhances the virulence of Shigella spp. and enteroinvasive Escherichia coli.* Proc Natl Acad Sci U S A, 1998. **95**(7): p. 3943-8.
49. Smith, E.E., et al., *Genetic adaptation by Pseudomonas aeruginosa to the airways of cystic fibrosis patients.* Proc Natl Acad Sci U S A, 2006. **103**(22): p. 8487-92.
50. Rancati, G., et al., *Aneuploidy underlies rapid adaptive evolution of yeast cells deprived of a conserved cytokinesis motor.* Cell, 2008. **135**(5): p. 879-93.
51. Gourguechon, S., L.J. Holt, and W.Z. Cande, *The Giardia cell cycle progresses independently of the anaphase-promoting complex.* J Cell Sci, 2013. **126**(Pt 10): p. 2246-55.

52. Akiyoshi, B. and K. Gull, *Discovery of unconventional kinetochores in kinetoplastids.* Cell, 2014. **156**(6): p. 1247-58.
53. Kwon, M.J., et al., *Functional characterization of Rho GTPases in Aspergillus niger uncovers conserved and diverged roles of Rho proteins within filamentous fungi.* Mol Microbiol, 2011. **79**(5): p. 1151-67.
54. Harris, S.D., *Cdc42/Rho GTPases in fungi: variations on a common theme.* Mol Microbiol, 2011. **79**(5): p. 1123-7.
55. Drinnenberg, I.A., et al., *Recurrent loss of CenH3 is associated with independent transitions to holocentricity in insects.* Elife, 2014. **3**.
56. Gordon, J.L., K.P. Byrne, and K.H. Wolfe, *Additions, losses, and rearrangements on the evolutionary route from a reconstructed ancestor to the modern Saccharomyces cerevisiae genome.* PLoS Genet, 2009. **5**(5): p. e1000485.
57. Neme, R. and D. Tautz, *Phylogenetic patterns of emergence of new genes support a model of frequent de novo evolution.* BMC Genomics, 2013. **14**: p. 117.
58. Neme, R. and D. Tautz, *Evolution: dynamics of de novo gene emergence.* Curr Biol, 2014. **24**(6): p. R238-40.
59. SGD, *Based on interaction maps.* www.yeastgenome.org.
60. Koh, J.L., et al., *DRYGIN: a database of quantitative genetic interaction networks in yeast.* Nucleic Acids Res, 2010. **38**(Database issue): p. D502-7.
61. Pan, X., et al., *A robust toolkit for functional profiling of the yeast genome.* Mol Cell, 2004. **16**(3): p. 487-96.
62. Wickerham, L.J., *Recent advances in the taxonomy of yeasts.* Annu Rev Microbiol, 1952. **6**: p. 317-32.
63. Sheff, M.A. and K.S. Thorn, *Optimized cassettes for fluorescent protein tagging in Saccharomyces cerevisiae.* Yeast, 2004. **21**(8): p. 661-70.
64. Sherman, F., Fink, G., and Lawerence, C., *Methods in Yeast Genetics.* (New York:
65. Gresham, D., et al., *The repertoire and dynamics of evolutionary adaptations to controlled nutrient-limited environments in yeast.* PLoS Genet, 2008. **4**(12): p. e1000303.

Figures

Figure 1 (with cartoon)**:** *BEM1* is an important polarity gene. A) Cartoon showing the components of the machinery for cell polarization relevant for this work. B) Images of two plates where 10^5 wild-type (left) versus 10^5 *bem1*Δ spores were plated. C) Differential interference contrast (DIC) images of *bem1*Δ and wild-type cells that grew from a single spore, showing that *bem1*Δ cells do not polarize effectively and therefore grow very large compared to wild type. Scale bar indicates 20 μm. D) Histograms of the time between

cytokinesis and bud formation for *bem1*Δ and wild-type cells that were born after germination from spores.

Figure 1 - figure supplement 1 DIC microscopy image of a microcolony that grew from a single *bem1*Δ cell that was taken from the colony that was used to start the experimental evolution experiment of the A-lines. Scale bar indicates 20 μm.

Figure 2 Experimental evolution experiments reveal that *bem1*Δ cells can adapt to wild-type growth rate and cell shape in 1000 generations. A) Cartoon of experimental evolution of *bem1*Δ and wild-type for 1000 generations by 100 cycles of serial dilution. B) The log phase growth rate in bulk was measured for several time points (in number of generations) of the evolution experiment, for different *bem1*Δ (A1-10) and wild-type lines. The insert shows that the growth rates of *bem1*Δ cells are close to, but in aggregate significantly lower (t-test, P-value < 1e-5) than the growth rate of wild-type cells at the end of the evolution experiment. C) DIC images of wild-type cells (left) and *bem1*Δ cells from line A1 at 30 (middle) and 1000 generations (right), showing changes in cell sizes within and between populations. D) Cell size distribution for wild-type cells (red) and *bem1*Δ cells from line A1 at 30 (dashed, purple) and 1000 generations (solid, purple).These data are fitted to a lognormal distribution to find the mode (peak location) and standard deviation. Subsequently, the mode (E) and standard deviation (F) are plotted for several time points of the evolution experiment for *bem1*Δ (A1-10) and wild-type lines. Note that the mode and standard deviation significantly increased in one of the wild-type lines due to increased clumping (Figure 2- figure supplement 1). The error bars indicate SD between independent experiments.

Figure 2 - figure supplement 1 Variable clumpiness in the evolved wild-type lines. A) Data as in figure 2E, where the mode is plotted for several time points of the evolution experiment for *bem1*Δ (A1-10) and wild-type lines. The ancestor (red) as well evolved line 1 (green) and

4 (purple) are highlighted. From the ancestor (B) as well as line 1 (C) and 4 (D) at 1000 generations, cells are imaged in log-phase with DIC microscopy, to visualize clumpiness. The red circles mark clumps of cells with three or more cells. E) Data from Figure 2, Figure 3 and Figure 4 are combined to show that cell size is an reasonable approximation for polarization time. The mode of the cell size for wildtype and line A1 is plotted at 30, 500 and 1000 generations on the x-axis. These time points represent mutants that subsequently dominate the population (Figure 3B), 30 gen ≈ *bem1Δ bem3Δ*, 500 gen ≈ *bem1Δ bem3Δ nrp1Δ*, 1000 gen ≈ *bem1 Δbem3 Δnrp1 bem2Δ*. We recreated these mutants in the presence of a polarity marker to measure polarization times (Figure 4), which is plotted on the Y axis. The plot indeed suggests a linear relation between cell size and polarization time. For details on polarization time measurements and the reconstruction see Figure 4 and the Supplementary Information.

Figure 3 Three mutations produce adaptation to deletion of *BEM1*. A) Locations of the mutations in the three genes that were mutated at least three times. The purple color indicates different functional domains in the genes. The three genes and locations of the mutations are drawn roughly to scale. B) For *bem1*Δ line A1 and A2 the fraction of the mutant versus the wild-type allele in the population is plotted against the number of generations in the evolution experiment. C) We sporulated a diploid yeast strain (*BEM1/bem1*Δ*::KanMx, BEM3/bem3*Δ*::Nat, NRP1/nrp1*Δ*::HphMx* and *BEM2/bem2*Δ*::LEU2)*, to obtain all different combinations of mutations. Subsequently we spotted those spores on plates (insert) and measured for every genotype, the percentage of macroscopic colonies forming spores (error bar is statistical error) as well as the average radius of those colonies (the error bar is the standard deviation). D) The log phase growth rate in bulk (the error bar is the standard deviation) is measured for the reconstructed intermediates of *bem1*Δ cells in line A1 and A2 (dark blue). The red line indicates the effect of the three adaptive mutations in a wild-type background. For comparison the purple dots and line indicates the difference between the

growth rates of the evolved lines A1 (faster) and A2 (slower) at the end of the evolution experiment. E) Hypercube where the genotype is depicted by the location and the color in the quadrant. The different paths on the hypercube represent all the different trajectories between any two genotypes within this genotype space. The area of the square represents the growth rate of that genotype, as indicated by the gray scale bar square. The outer-cube represents all *BEM1* lines, which are in our evolutionary experiment inaccessible, because the *BEM1* gene was completely removed from the genome, however this data is included to reveal the relative change in *BEM1* dependence in different genetic backgrounds.

Figure 3 - figure supplement 1 Reconstructing the evolutionary trajectory. (A) Cartoon showing how sporulation of a heterozygous diploid results in haploids with all the different combinations of gene knock outs. Only eight of the sixteen genotypes are shown. B) Image of a plate where we spotted individual spores from the heterozygous diploid. We measured the colony size from 810 spores deposited on ten plates in a 9x9 grid using automated image analysis. Afterwards we determined the genotype of the spores by replica plating them to different selective media as shown in (C), which allowed us to calculate the percentage of surviving colonies by diving the number of observed spores by the number of expected spores (50 per genotype). Afterwards we took cells with different genotypes from these plates to measure their growth rate in log-phase in liquid media, as well as for microscopic analysis (Figure 4).

Figure 4 Three adaptive mutations change polarization dynamics to re-establish efficient polarization. A) Z-projections of spinning disk fluorescence microscopy images of Spa2-Citrine, which marks the site of polarization as well as the cytokinetic ring, in yeast cells at different reconstructed stages of the evolution. The scale bar indicates 10 μm. B) Cartoon explaining our analysis of polarization dynamics. For the indicated number of mother cells (N) we average 1) the time ($t_{fs\text{-}c}$) between cytokinesis (t_c) and the moment that the first

polarity spot appears (t_{fs}), indicated in red, and 2) the total time per cell cycle, after t_{fs}, when cells contained zero, one, two or three polarity spots (for details see supplementary materials). The different times are combined in a horizontal bar plot (C) where the length of the bars indicates the average time in minutes.

Video's

Video 1: DIC microscopy movie of germinating spores (time step is 3min) growing in a micro fabricated channel with constant media supply. The spore in the bottom-left is wild-type and the spore in the top-right is *bem1*Δ. The movie plays at 2520x real time and the time stamps show hh:mm.

Video 2: DIC microscopy movie of a microcolony that grew from an individual *bem1*Δ spore (time step is 3min) in a micro-fabricated channel with constant media supply. Both very large cells, which often lyse, and small, fast dividing cells can be observed. The movie plays at 2520x real time and the time stamps show hh:mm.

Video 3: DIC microscopy movie of a microcolony that grew from an individual *bem1*Δ cell, taken from the same colony that was used for the large evolution experiment (A lines). The colony was grown on an agar pad to provide constant culturing conditions (time step is 2 min). The movie plays at 2520x real time and the time stamps show hh:mm.

Video 4: Spinning disk confocal fluorescence microscopy movie of Spa2-Citrine in wild type cells. For every image the cells were exposed for 200ms with a 488 laser (the time step is 2 min). The movie shows a time series of maximum projections of 7 z-stacks (z-step is 1μm). For Videos 4 to 8, the image size and the intensity values are kept constant. The cells are grown in a micro-fabricated channel with constant media supply. As cells divide, Spa2 concentrates at the bud neck and the single fluorescent focus splits in two with both mother and daughter cells inheriting localized Spa2. In mothers this spot often becomes the site where

buds emerge, but in daughters, who spend longer in G1, the spot typically disappears and later reappears, at a different site, just before the next bud emerges. The movie plays at 2520x real time and the time stamps show hh:mm.

Video 5: Cell polarization in *bem1*Δ cells. Conditions are identical to Video 4; however the cells in the movie are *bem1*Δ. Note the much slower cell cycles, the appearance and disappearance of Spa2 spots that do not give rise to budding, including one site of Spa2 accumulation that persists for most of the movie, but does not lead to a bud emerging. Cells rarely show two simultaneous strong Spa2 spots. The movie plays at 2520x real time and the time stamps show hh:mm.

Video 6: Cell polarization in *bem1*Δ *bem3*Δ cells. Conditions are identical to Video 4; however the cells in the movie are *bem1*Δ *bem3*Δ double mutants. Note the frequent presence of two competing spots of localized Spa2. The movie plays at 2520x real time and the time stamps show hh:mm.

Video 7: Cell polarization in *bem1*Δ *bem3*Δ *nrp1*Δ cells. Conditions are identical to Video 4; however the cells in the movie are *bem1*Δ *bem3*Δ *nrp1*Δ triple mutants. Competition between competing Spa2 spots is resolved more quickly than in *bem1*Δ *bem3*Δ cells. The movie plays at 2520x real time and the time stamps show hh:mm.

Video 8: Cell polarization in *bem1*Δ *bem3*Δ *nrp1*Δ *bem2*Δ cells. Conditions are identical to Video 4; however the cells in the movie are *bem1*Δ *bem2*Δ *bem3*Δ *nrp1*Δ quadruple mutants. Although these cells bud at similar sizes and rates as *BEM1* cells, some cells show prolonged presence of two or more Spa2 spots and mothers rarely produce their next bud close to the site of its predecessor. The movie plays at 2520x real time and the time stamps show hh:mm.

Supplementary Files:

Supplementary File 1: Mutations in the evolved lines.

Supplementary File 2: Yeast strains.

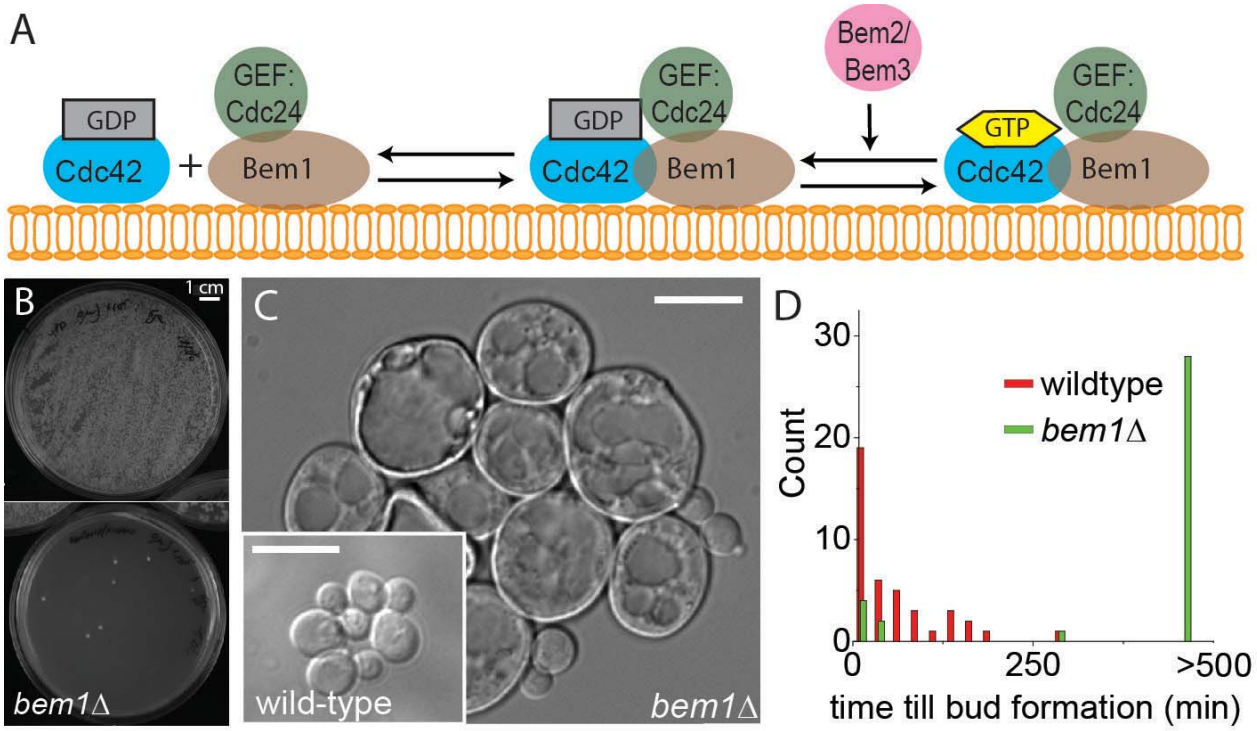
A
GDP
Cdc42
+
GEF:
Cdc24
Bem1
GDP
Cdc42
GEF:
Cdc24
Bem1
Bem2/
Bem3
GTP
Cdc42
GEF:
Cdc24
Bem1
B
1 cm
bem1Δ
C
wild-type
bem1Δ
D
Count
30
20
10
0
0
250
>500
wildtype
bem1Δ
time till bud formation (min)

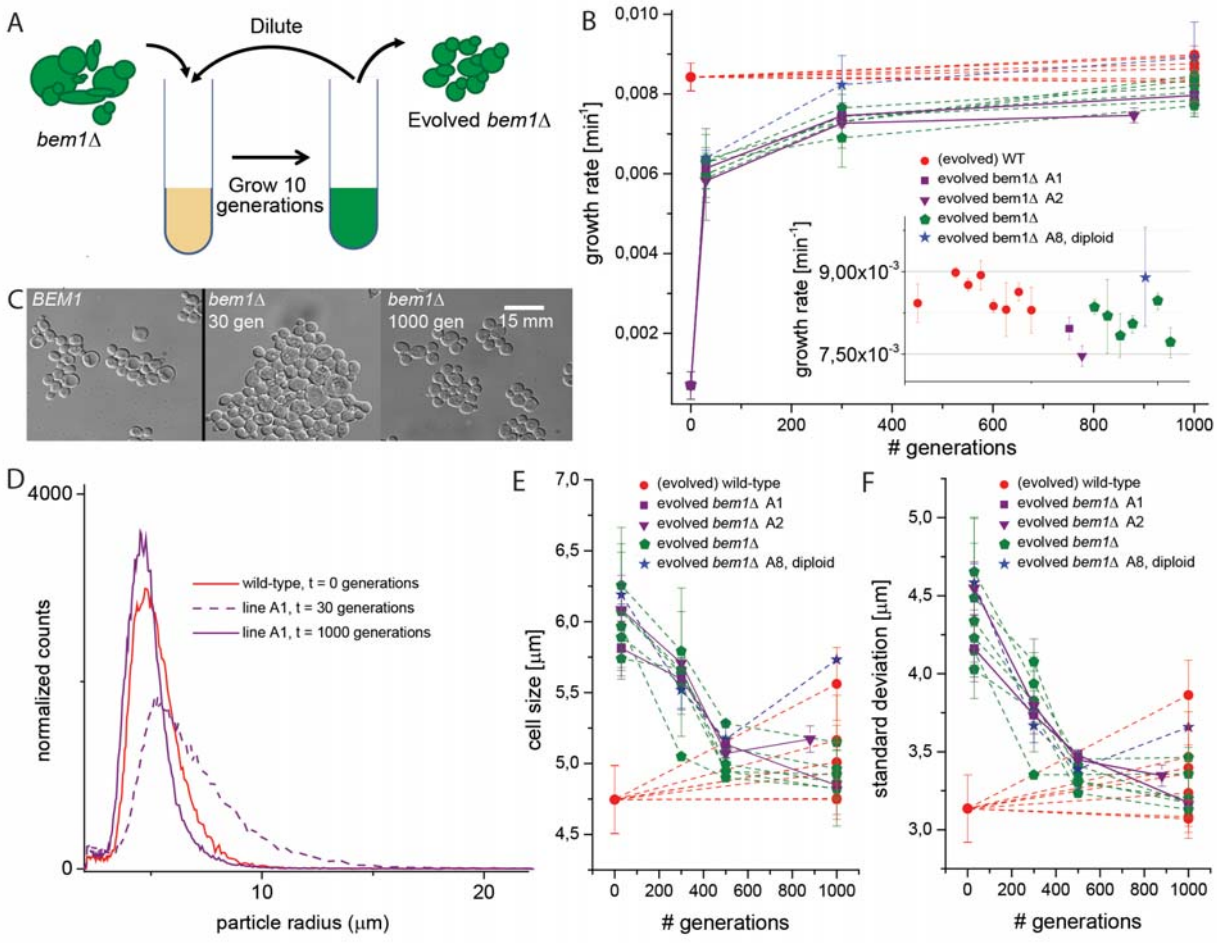
A
Dilute
bem1Δ
Evolved bem1Δ
Grow 10 generations
B
growth rate [min-1]
generations
(evolved) WT
evolved bem1Δ A1
evolved bem1Δ A2
evolved bem1Δ
evolved bem1Δ A8, diploid
9,00x10-3
7,50x10-3
C
BEM1
bem1Δ 30 gen
bem1Δ 1000 gen
15 mm
D
normalized counts
wild-type, t = 0 generations
line A1, t = 30 generations
line A1, t = 1000 generations
particle radius (μm)
E
cell size [μm]
generations
F
standard deviation [μm]
generations

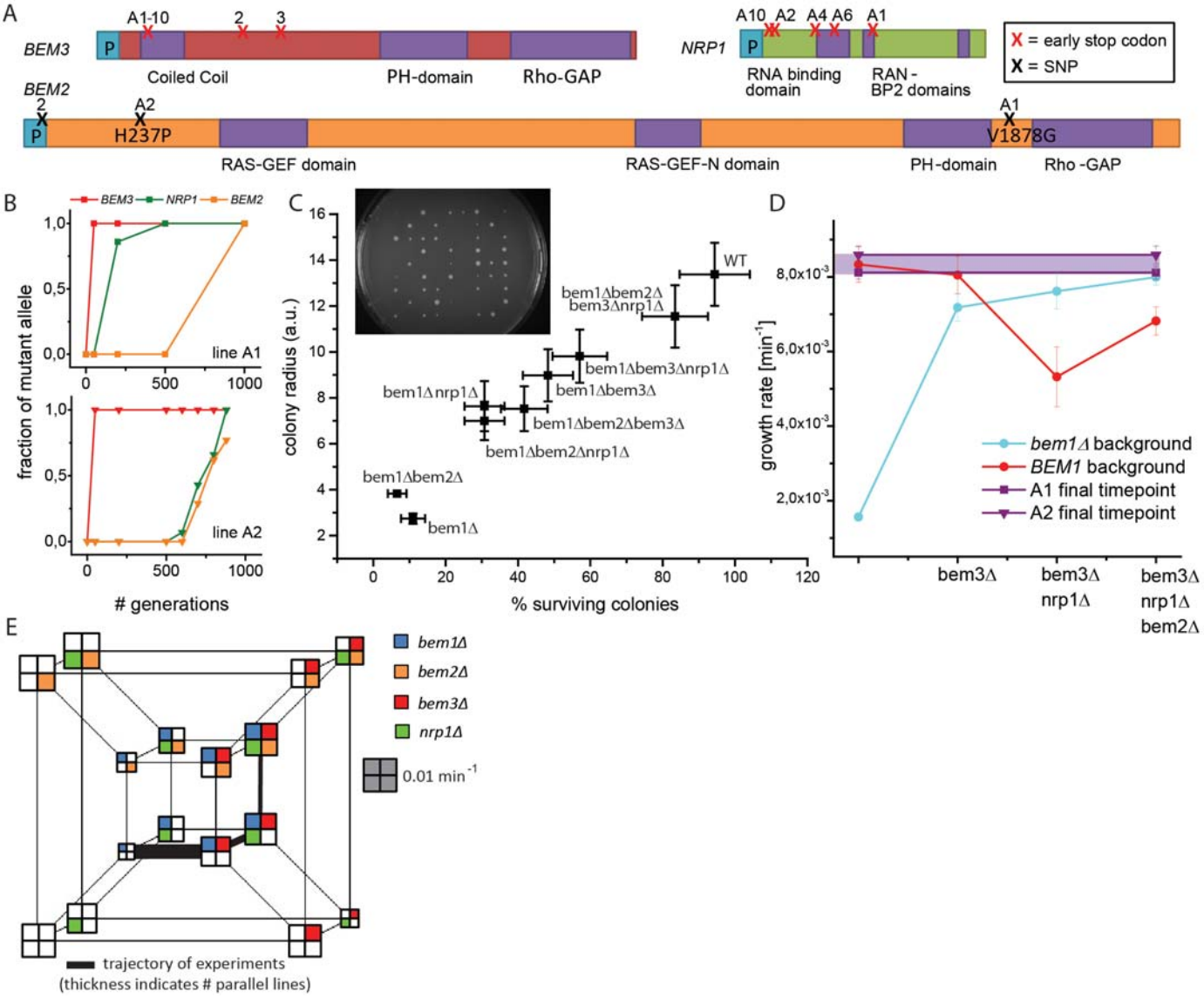
A
BEM3
P
A1-10
2
3
Coiled Coil
PH-domain
Rho-GAP
NRP1
P
A10 A2 A4 A6 A1
RNA binding domain
RAN - BP2 domains
X = early stop codon
X = SNP
BEM2
2
A2
P
H237P
A1
V1878G
RAS-GEF domain
RAS-GEF-N domain
PH-domain
Rho -GAP
B
BEM3 NRP1 BEM2
fraction of mutant allele
line A1
line A2
generations
C
colony radius (a.u.)
% surviving colonies
WT
bem1Δbem2Δ
bem3Δnrp1Δ
bem1Δbem3Δnrp1Δ
bem1Δbem3Δ
bem1Δnrp1Δ
bem1Δbem2Δbem3Δ
bem1Δbem2Δnrp1Δ
bem1Δbem2Δ
bem1Δ
D
growth rate [min-1]
bem1Δ background
BEM1 background
A1 final timepoint
A2 final timepoint
bem3Δ
bem3Δ nrp1Δ
bem3Δ nrp1Δ bem2Δ
E
bem1Δ
bem2Δ
bem3Δ
nrp1Δ
0.01 min-1
trajectory of experiments
(thickness indicates # parallel lines)

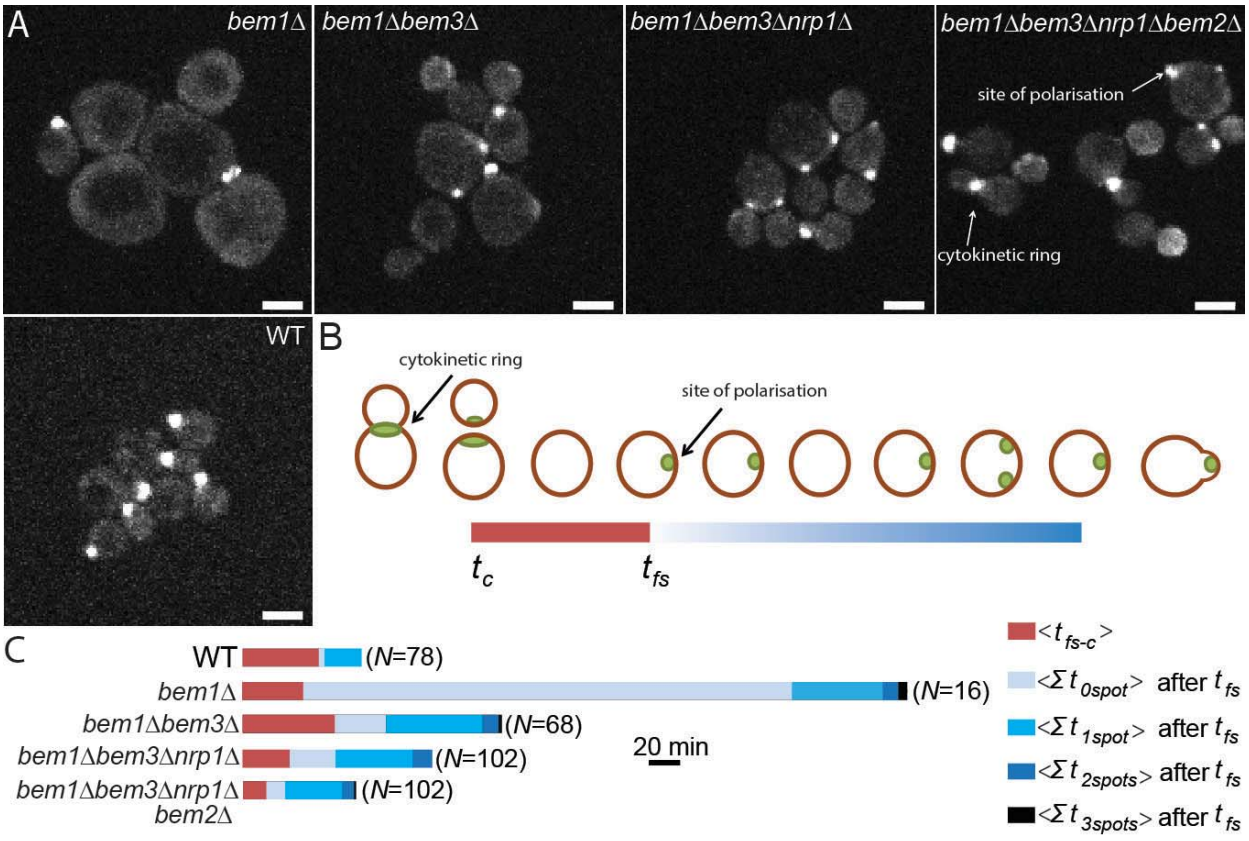
A
bem1Δ
bem1Δbem3Δ
bem1Δbem3Δnrp1Δ
bem1Δbem3Δnrp1Δbem2Δ
site of polarisation
cytokinetic ring
WT
B
cytokinetic ring
site of polarisation
t_c
t_{fs}
C
WT (N=78)
bem1Δ (N=16)
bem1Δbem3Δ (N=68)
bem1Δbem3Δnrp1Δ (N=102)
bem1Δbem3Δnrp1Δ bem2Δ (N=102)
20 min
$<t_{fs-c}>$
$<\Sigma t_{0spot}>$ after t_{fs}
$<\Sigma t_{1spot}>$ after t_{fs}
$<\Sigma t_{2spots}>$ after t_{fs}
$<\Sigma t_{3spots}>$ after t_{fs}